23
Lubrication

A cylindrical shaft rotating in a bush lies behind *the* most important technological invention, the wheel and its bearing. From the earliest times it was realized that friction in the bearing was considerably lowered by lubricating it with viscous fluid. Wooden bearings might even catch fire if not lubricated. Fat from pigs, olive oil and mineral oil turned out to work much better than water.

When you deal a pack of cards on a table with a smooth surface, it is easy to overestimate the speed the cards must be thrown with. Suddenly, several cards in a row slide easily over the surface and land on the floor. The reason is that a lubricating layer of air has formed between the card and the surface of the table, and has caused the friction you expected when throwing the card, to drop away. Air also lubricates the tiny gap between the magnetic pickup heads and the rapidly spinning harddisk in your computer and prevents the heads from crashing into the surface. Water is used to lubricate children's slides in amusement parks, and sports like ice skating or curling depend crucially on a thin lubricating film of water.

In this chapter we shall analyze incompressible flow in narrow gaps along the lines laid out by Reynolds already in 1886. As the fluid-filled gap between a moving object and a nearby solid surface narrows, viscosity plays an increasingly dominant role, because the velocity gradients normal to the surface grow large compared to the gradients parallel to the surface. Sufficiently close to the surface the effective Reynolds number for the flow in the gap may become so small that the approximation of creeping flow is appropriate. If the gap widens towards the front of the moving object, as is mostly the case, fluid will be forced into the gap, creating a pressure that can become surprisingly high. As the gap narrows, the lift from this pressure will in the end become sufficient to keep the object afloat in the lubricant, thereby securing a smooth ride.

Copyright © 1998–2002, Benny Lautrup

23.1 Lift and drag near a boundary

Far from any boundaries, the flow around an object of size L moving with velocity U through an otherwise stationary fluid of density ρ and viscosity η is characterized by the Reynolds number

$$\mathsf{Re} \approx \frac{\rho U L}{\eta} \tag{23-1}$$

In many everyday situations — running, swimming, driving, washing dishes or babies — the Reynolds number is very large, $\mathsf{Re} \gg 1$, and the flow may be considered nearly ideal (see chapter 15).

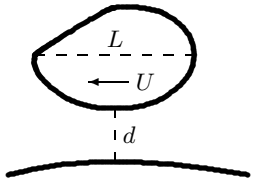

Object moving close to a nearly planar boundary. The gap is assumed to be so narrow that creeping flow conditions prevail.

A body moving with velocity U near a stationary solid boundary will generate large fluid stresses, because the no-slip condition forces the fluid velocity to change from 0 to U across the narrow gap between the body and the boundary. The typical width d of the gap is assumed to be much smaller than the extent L of the body, $d \ll L$, and the body is assumed to have a reasonably smooth surface without sharp protrusions, such that the width only varies slowly along the gap.

Condition for creeping flow

The effective Reynolds number in the gap may as usual be estimated from the actual ratio between the advective and viscous forces

$$\frac{|\rho(\boldsymbol{v}\cdot\boldsymbol{\nabla})\boldsymbol{v}|}{|\eta\boldsymbol{\nabla}^2\boldsymbol{v}|} \approx \frac{\rho U^2/L}{\eta U/d^2} = \left(\frac{d}{L}\right)^2 \mathsf{Re}\ . \tag{23-2}$$

Whereas the numerator is characterized by the velocity derivative along the gap, the Laplacian in the denominator is completely dominated by the double derivatives across the gap. The estimate shows that even if the free-flow Reynolds number (23-1) is large, viscous forces will dominate the flow in the gap when the distance d becomes sufficiently small. This happens for $d \lesssim \delta$ where

$$\boxed{\delta = \frac{L}{\sqrt{\mathsf{Re}}}}\ . \tag{23-3}$$

In chapter 24 we shall see that δ is a measure of the thickness of the boundary layer that surrounds a moving body. The above inequality thus shows that the conditions for creeping flow are fulfilled when the gap lies well inside the boundary layer.

Example 23.1.1: A playing card roughly 10 cm in size skimming through the air over a table at roughly 1 m s^{-1}, has $\mathsf{Re} \approx 10^4$ and thus $\delta \approx 1$ mm. The condition for creeping flow is fulfilled when the distance to the table is somewhat less than δ, for example 0.3 mm.

Copyright © 1998–2002, Benny Lautrup

Lift

If the boundary is assumed to be planar and moving with velocity U, whereas the body is stationary, we may as before use the equations for steady creeping flow (22-1). The flow in the gap will generate a pressure force, or *lift* $\mathcal{L}$, that may drive the body away from (or towards) the boundary. The magnitude of the lift can be estimated from the field equation for creeping flow, $\boldsymbol{\nabla} p = \eta \boldsymbol{\nabla}^2 \boldsymbol{v}$. Since the double derivatives orthogonal to the flow dominate the Laplacian, we estimate $|\boldsymbol{\nabla} p| \approx \eta U/d^2$. Multiplying with the length of the gap, L, we obtain the magnitude of the pressure variations along the gap, $|\Delta p| \approx \eta U L/d^2$. Finally multiplying with the gap area A, we get for the lift

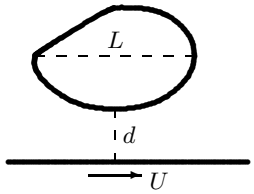

In the reference frame where the boundary moves with velocity U, the object is stationary.

$$\mathcal{L} \approx f \frac{\eta U L A}{d^2} \ , \tag{23-4}$$

where f is a dimensionless prefactor, depending on the orientation of the body and expected to be at most of order unity. The flow around around the upper part of the body will also cause lift, but the lift from the fluid in the gap will always dominate in the limit of $d \to 0$, because of the denominator.

For simplicity we shall assume that the underside of the body is reasonably flat, forming an *angle of attack* α with the boundary. The sign of this angle is chosen to be positive when the gap widens towards the front of the body, and intuitively one expects in this case a positive lift that drives the body away from the boundary. For vanishing angle of attack, the flow will essentially become planar velocity-driven Couette flow (see page 287), and no lift is generated. For negative angle of attack the lift is expected to be negative, causing the body be sucked towards the boundary rather than pushed away from it.

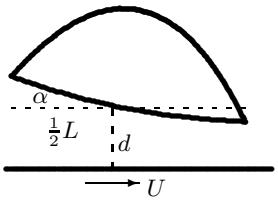

Body with relatively flat underside and a small positive angle of attack α. In this case the lift will be upwards. The rear of the body will touch the ground at the rear if $\alpha \frac{1}{2} L \approx d$ where d is the average width.

These arguments indicate that the prefactor in the leading approximation should be proportional to the angle of attack, $f \sim \alpha$. Taking into account that the magnitude of this angle is limited by the requirement that the body should not touch the ground, *i.e.* $|\alpha| \lesssim 2d/L$, we estimate that

$$f \approx \alpha \frac{L}{2d} \ . \tag{23-5}$$

The calculations in section 23.3 will confirm that this estimate is essentially correct.

Example 23.1.2: A playing card with mass $M \approx 1$ gram and length $L \approx 10$ cm is thrown with velocity $U = 1$ m s^{-1} over the surface of a table. Provided the table surface is smooth, the card will sink into the boundary layer and get sufficient lift to fly without ever touching the table. Taking the shape factor $f \approx 0.1$, the lift equals the weight for $d \approx 0.3$ mm. The corresponding angle of attack becomes $\alpha \approx 0.3^\circ$. The card probably has to bend slightly upwards for steady lift to be generated. Professional card players avoid bending their cards and also cover the table with rough green felt cloth. You never see a card skimming the table surface and land on the floor in their company.

Copyright © 1998–2002, Benny Lautrup

Skin drag

In the gap the orthogonal velocity gradient is U/d, so that the shear stress becomes $\sigma \approx \eta U/d$. Multiplying with the effective area A of the gap, we obtain an estimate for the *skin drag* on the body from fluid friction in the gap,

$$\mathcal{D}_{\mathsf{skin}} \approx \sigma A \approx \frac{\eta U A}{d} \ . \tag{23-6}$$

The linear variation with velocity is as discussed before (section 22.1) characteristic of creeping flow. As for lift, there will also be drag from the flow around the body outside the gap, but the drag from the fluid in the gap will always dominate over other drag in the limit of $d \to 0$, because of the denominator.

Both lift and skin drag grow with decreasing gap size, but the lift grows faster than the drag and eventually comes to dominate it. The ratio of lift to skin drag is estimated by

$$\frac{\mathcal{L}}{\mathcal{D}_{\mathsf{skin}}} \approx f\frac{L}{d} \approx \frac{1}{2}\alpha\left(\frac{L}{d}\right)^2 \ . \tag{23-7}$$

This shows that if the angle of attack is sufficiently small, $\alpha \lesssim 2(d/L)^2$, the drag may actually dominate the lift, but that requires careful tuning of the angle of attack, which is usually not possible.

Example 23.1.3: For the playing card of example 23.1.2, the actual ratio of lift to skin drag is $\mathcal{L}/\mathcal{D}_{\mathsf{skin}} \approx 30$. They would become equal for $f \approx d/L$, and from the balance of lift (23-4) and weight Mg_0, we get the flying height $d \approx 20$ $\mu\mathsf{m}$. The corresponding angle of attack becomes minuscule, $\alpha \approx 5 \times 10^{-6}$ degrees.

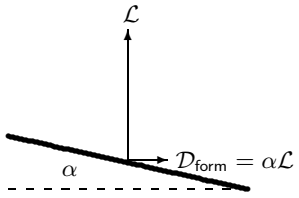

The pressure acts orthogonally to the surface and gives rise to vertical lift as well as horizontal form drag.

Form drag

Besides frictional skin drag there will also be a *form drag* from the pressure variations in the gap. The form drag may be estimated from the angle of attack and the lift,

$$\mathcal{D}_{\mathsf{form}} \approx \alpha\mathcal{L} \ . \tag{23-8}$$

Since the lift itself is proportional to α, the form drag will always be positive, independently of the sign of α. Drag forces should, of course, never be able to accelerate a body.

Contrary to the skin drag, which (to leading order) is independent of the angle of attack, the form drag is quadratic in α and vanishes for $\alpha = 0$. Using the estimates above we obtain the ratio of form to skin drag

$$\frac{\mathcal{D}_{\mathsf{form}}}{\mathcal{D}_{\mathsf{skin}}} \approx \alpha f\frac{L}{h} \approx 2f^2 \ . \tag{23-9}$$

Since this is at most of order unity, we conclude that although the form drag for fixed α varies like $1/h^3$, it can never really win over skin drag because of the geometrical constraints.

Copyright © 1998–2002, Benny Lautrup

Example 23.1.4: Magnetic read/write head design. The continued sophistication in the design of read/write heads and platter surfaces has been a major cause for the enormous improvement in harddisk performance over the last 30 years. A typical modern (2002) harddisk has a diameter of about 9 cm and runs at a speed of about 7,000 rpm, leading to average platter surface speeds of $U \approx 16$ m s^{-1} ≈ 60 km h^{-1}. The read/write heads sit on the tip of an actuator arm that can roam over the rotating platters and exchange data with the magnetic surfaces. A typical read/write head is formed as a flat wing or "slider" with size $L \approx 1$ mm, for which the Reynolds number comes to about $\mathsf{Re} \approx 1,000$, and the maximal gap size for creeping flow comes to $\delta \approx 30$ μm. The need for increased data density demands smaller and smaller flying height for the heads. Today the typical flying height is $d \approx 0.15$ μm (and even smaller), implying that the head flies deeply inside the boundary layer. At this height the maximal angle of attack becomes $\alpha_{\max} = 2d/L \approx 0.017$ degrees, and assuming $f = 0.3$, the actual angle of attack is $\alpha \approx 0.005$ degrees. The lift force on the head becomes $\mathcal{L} \approx 4$ N, corresponding to a weight of 400 g, which must be provided by the elastic actuator arm. The ratio of form to skin drag is $\mathcal{D}_{\mathsf{form}}/\mathcal{D}_{\mathsf{skin}} \approx 0.2$ and the ratio of lift to skin drag $\mathcal{L}/\mathcal{D}_{\mathsf{skin}} \approx 2000$. The average excess pressure in the gap becomes surprisingly high, $\Delta p \approx \mathcal{L}/A \approx 4 \times 10^6$ Pa $= 40$ bar, and this actually invalidates the tacit assumption of incompressible flow that we have made in the estimates.

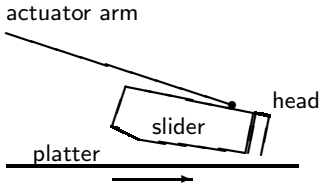

Sketch of the head-to-disk interface in a harddisk. The platter rotates towards the left and drags air into the gap between the slider and the surface, and thereby prevents the slider from touching the platter. The elastic actuator arm counteracts the lift force from the air in the gap. The head itself is here positioned at the rear end of the slider.

23.2 Flow in a narrow gap

Creeping 'flight' near a solid boundary is much more amenable to analytic calculations than real aerodynamics (see chapter 26). For simplicity we shall disregard the third dimension and consider an essentially infinitely long stationary two-dimensional 'wing' and choose a coordinate system with the z-axis along the wing. The ground is chosen to be perfectly flat, given by $y = 0$ for all x (and z), moving with constant velocity U along x. The height of the wing above the ground is $y = h(x)$ (for all z). It should be small enough for the creeping approximation to be valid everywhere in the gap, and it should vary slowly along the gap, *i.e.* $|\alpha(x)| \ll 1$. The local angle of attack $\alpha(x) = -h'(x)$ must in other words be small.

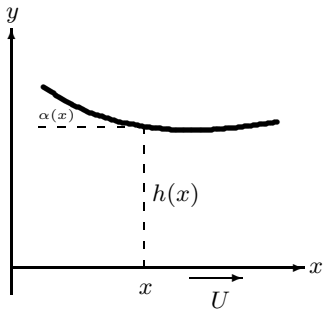

Local geometry of creeping 'flight'. The 'ground' and the 'air' move with velocity U relative to the 'wing' which flies at height $y = h(x)$. The local angle of attack is $\alpha(x) = -h'(x)$.

The gap equations

Keeping only the dominant derivatives after y in the Laplacian of (22-1), we obtain the simplified equations for the flow in the gap,

$$\frac{\partial p}{\partial x} = \eta \frac{\partial^2 v_x}{\partial y^2} \ , \tag{23-10a}$$

$$\frac{\partial p}{\partial y} = \eta \frac{\partial^2 v_y}{\partial y^2} \ , \tag{23-10b}$$

$$\frac{\partial v_y}{\partial y} = -\frac{\partial v_x}{\partial x} \ . \tag{23-10c}$$

where the last is the continuity equation.

Copyright © 1998–2002, Benny Lautrup

The second equation (23-10b) may be solved immediately with the result

$$p(x,y) = P(x) + \eta\frac{\partial v_y(x,y)}{\partial y} = P(x) - \eta\frac{\partial v_x(x,y)}{\partial x} \ , \tag{23-11}$$

where $P(x)$ is an arbitrary function that is independent of x. Inserting this in (23-10a) and dropping again the second order derivative of v_x after x, we obtain

$$\boxed{\eta\frac{\partial^2 v_x(x,y)}{\partial y^2} = P'(x)} \ . \tag{23-12}$$

With boundary conditions $v_x = U$ at $y = 0$ and $v_x = 0$ at $y = h(x)$, the solution is

$$v_x(x,y) = \frac{U}{h(x)}(h(x) - y) - \frac{P'(x)}{2\eta}y(h(x) - y) \ . \tag{23-13}$$

For any x, the solution is basically velocity-driven planar flow (17-3) superposed with pressure-driven planar flow (18-8). The only difference is that now the plate distance $h(x)$ and the pressure gradient $P'(x)$ may both vary with x.

Solution

The moving "ground" at $y = 0$ drags fluid in the direction of positive x. The total discharge rate Q (per unit of length in the z-direction) becomes,

$$Q = \int_0^{h(x)} v_x(x,y)\,dy = \frac{1}{2}Uh(x) - \frac{P'(x)h(x)^3}{12\eta} \ . \tag{23-14}$$

But Q must be independent of x because of the incompressibility of the fluid, so that we may solve for the pressure gradient

$$\boxed{P'(x) = 6\eta\left(\frac{U}{h(x)^2} - \frac{2Q}{h(x)^3}\right)} \ . \tag{23-15}$$

For a given gap shape $h(x)$ this may be integrated to get the pressure. Eliminating the pressure gradient in the velocity, we find

$$\boxed{v_x = U\frac{(h-y)(h-3y)}{h^2} + Q\frac{6y(h-y)}{h^3}} \ . \tag{23-16}$$

Here we have for clarity suppressed the explicit dependence on x which is now entirely due to the slowly varying gap height $h(x)$. Finally, we insert v_x into the continuity equation (23-10c) and integrate over y with the boundary condition $v_y = 0$ for $y = 0$, to obtain

$$\boxed{v_y = 2\alpha\left(\frac{U}{h^3} - \frac{3Q}{h^4}\right)y^2(h-y)} \ , \tag{23-17}$$

where $\alpha(x) = -h'(x)$ is the local angle of attack.

Copyright © 1998–2002, Benny Lautrup

Flow reversal

The discharge rate Q must be proportional to the ground velocity U because of the linearity of the equations of creeping flow (22-1). The actual relation between Q and U depends on the shape of the gap. For a flat plate with constant gap height, $h(x) = d$, the planar flow solution (17-3) yields $Q = Ud/2$. In the general case it is convenient to define the parameter

$$h_0 = \frac{2Q}{U} \ , \tag{23-18}$$

which has dimension of length. It represents the equivalent height of a planar gap that would carry the same discharge rate as the actual gap, and is related but not equal to the average gap height d.

The pressure gradient may now be written

$$P' = \frac{6\eta U}{h^2}\left(1 - \frac{h_0}{h}\right) \ , \tag{23-19}$$

and we conclude that in regions where the gap height $h(x)$ is greater than h_0, the pressure will rise, whereas it will fall in regions where $h(x)$ is smaller. Intuitively, we expect h_0 to be larger than the smallest gap height, implying that there will always be a region with negative pressure gradient.

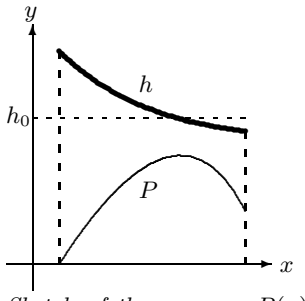

Sketch of the pressure $P(x)$ under the wing in relation to h_0.

Then the 'horizontal' velocity field may similarly be written

$$v_x = U\left(1 - \frac{y}{h}\right)\left(1 - \frac{3y}{h}\left(1 - \frac{h_0}{h}\right)\right) \ . \tag{23-20}$$

Evidently the last factor is positive for small y, but may vanish and become negative at $y = y_0$, where

$$y_0 = \frac{1}{3}\frac{h}{1 - \dfrac{h_0}{h}} \ . \tag{23-21}$$

When this point happens to lie in the gap, *i.e.* for $0 < y_0 < h(x)$, the fluid close to the stationary plate will flow *against* the direction of ground motion . Evidently this is only possible for $1 - h_0/h > 1/3$, or

$$h(x) > \frac{3}{2}h_0 \tag{23-22}$$

In regions where flow reversal occurs, "rollers" of counter-rotating fluid will appear. Typically, this happens when the gap widens locally. Since the discharge rate is mostly determined by the narrow parts of the gap, the equivalent height h_0 will be considerably lower than the maximal height of the bump, permitting the above inequality to be fulfilled. In the two following sections we shall find the explicit conditions for the appearance of flow reversal.

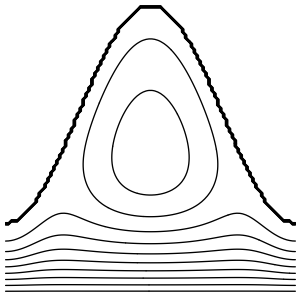

Pattern of flow reversal under a periodic wing given by $h(x) = 1 - 0.6\cos x$. A roller forms under each bump, here shown in the interval $0 \le x \le 2\pi$.

Copyright © 1998–2002, Benny Lautrup

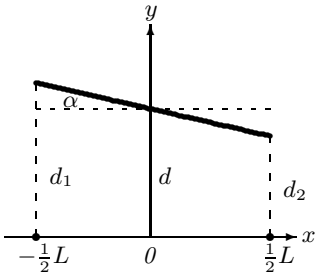

Geometry of flat wing with constant angle of attack α and average height d. Varying α rotates the wing around its midpoint.

23.3 Flat wing

Up to this point, everything has been valid for an arbitrary wing shape. We shall now specialize to the case of a flat wing with constant angle of attack α and average height d,

$$h(x) = d - \alpha\, x \ , \tag{23-23}$$

with $-L/2 \le x \le L/2$. Instead of the parameters α and d, it may be more convenient to specify the extreme heights, d_1 and d_2, at the front and back of the wing. The average height is then $d = (d_1 + d_2)/2$ and the angle of attack $\alpha = (d_1 - d_2)/L$. It is also convenient to define the dimensionless parameter

$$\gamma = \frac{\alpha L}{2d} = \frac{d_1 - d_2}{d_1 + d_2} \ , \tag{23-24}$$

which ranges over the interval, $-1 < \gamma < 1$.

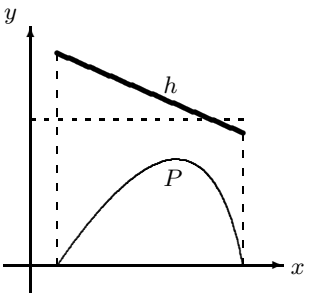

The pressure $P(x)$ under the flat wing has to be the same in front and in back, so that it has to rise and then fall back again.

Pressure and lift

The pressure gradient (23-15) may now immediately be integrated to

$$P(x) = P_0 + \frac{6\eta}{\alpha}\left(\frac{U}{h(x)} - \frac{Q}{h(x)^2}\right) \ , \tag{23-25}$$

where P_0 is a constant. The flat wing is assumed to fly in a fluid which would have constant pressure, were it not for the disturbance created by the wing itself. The pressure must for this reason be (nearly) the same in both ends of the wing, or $P(-L/2) = P(L/2)$, and this condition fixes the discharge rate to

$$Q = U\frac{d_1 d_2}{d_1 + d_2} = \frac{1}{2}Ud(1-\gamma^2) \ . \tag{23-26}$$

As expected, the discharge rate vanishes, if either end of the wing touches the ground, $|\gamma| = 1$. The constant P_0 is chosen such that the pressure vanishes at either end of the wing

$$P_0 = -\frac{6\eta U}{\alpha(d_1 + d_2)} \ . \tag{23-27}$$

The total lift from the gap pressure becomes for a wing of 'span' S and area $A = LS$,

$$\mathcal{L} = \int_{-L/2}^{L/2} P(x)\, S dx = \frac{\eta U L A}{d^2}\ \frac{3}{2\gamma^2}\left(\log\frac{1+\gamma}{1-\gamma} - 2\gamma\right) \ . \tag{23-28}$$

The γ-dependent factor on the right, called f in eq. (23-4), represents the influence of the shape and orientation of the wing. The lift changes sign under $\gamma \to -\gamma$ as expected, and converges for $\gamma \to 0$ on the estimate (23-5), $f = \gamma = \alpha L/2d$. The linear region where $f \approx \gamma$ extends over the interval $-0.7 < \gamma < 0.7$ and is a very good approximation in most cases of interest (see fig. 23.1).

Copyright © 1998–2002, Benny Lautrup

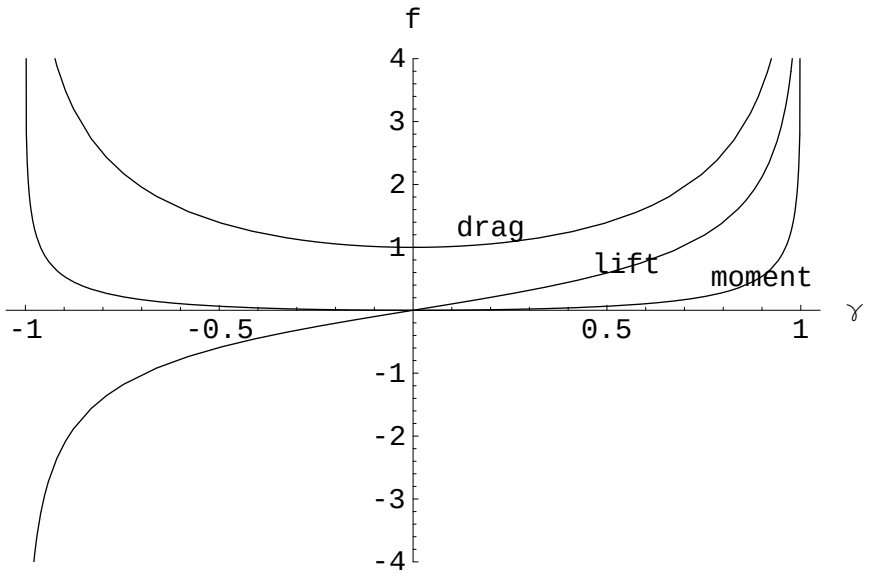

Figure 23.1: *Orientation-dependent shape factors for lift , drag and moment for a flat wing as a function of* $\gamma = \alpha L/2d$. *All quantities diverge logarithmically for* $|\gamma| \to 1$.

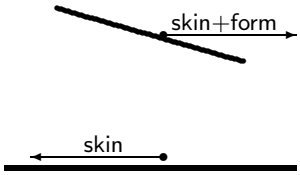

The drag on the wing is composed of skin and form drag, whereas the drag on the ground is only skin drag. Newton's third law guarantees that the total drag on the wing is equal and opposite the drag on the ground.

Drag

As discussed in section 23.1 the drag on the wing has two components, called skin drag arising from viscous friction and form drag arising from pressure forces projected on the direction of motion. The 'ground' also experiences a skin drag, but in this case the form drag vanishes because the ground is aligned with the direction of motion. Newton's third law tells us that the drag forces on the wing and on the ground must be equal and opposite, and this allows us to calculate the total drag on the wing, $\mathcal{D} = \mathcal{D}_{\mathsf{skin}} + \mathcal{D}_{\mathsf{form}}$, alone from the skin drag on the ground.

The shear stress on the flat ground is

$$\sigma_{xy}\big|_{y=0} = \eta \left[\frac{\partial v_x}{\partial y} + \frac{\partial v_y}{\partial x} \right]_{y=0} = -2\eta \left(\frac{2U}{h} - \frac{3Q}{h^2} \right) . \tag{23-29}$$

Integrating the shear stress over the ground surface, and changing sign in accordance with Newton's third law, we obtain the total drag on the wing,

$$\mathcal{D} = -\int_{-L/2}^{L/2} \sigma_{xy}\big|_{y=0} \, S dx = \frac{\eta U A}{d} \, \frac{1}{\gamma} \left(2 \log \frac{1+\gamma}{1-\gamma} - 3\gamma \right) . \tag{23-30}$$

The leading part of this expression agrees with the estimate (23-6). The drag estimate is modified by a γ-dependent factor which converges to unity for $\gamma \to 0$ and like the lift diverges logarithmically for $|\gamma| \to 1$ (see fig. 23.1). Since the form drag on a flat wing is $\mathcal{D}_{\mathsf{form}} = \alpha \mathcal{L}$, the skin drag can be found by subtracting the form drag from the total, $\mathcal{D}_{\mathsf{skin}} = \mathcal{D} - \mathcal{D}_{\mathsf{form}}$.

Copyright © 1998–2002, Benny Lautrup

Moment

The pressure forces create a turning moment around the center of the wing,

$$\mathcal{M} = \int_{-L/2}^{L/2} xP(x)\, S dx = \frac{\eta U L^2 A}{d^2}\ \frac{3}{8\gamma^3}\left((3-\gamma^2)\log\frac{1+\gamma}{1-\gamma} - 6\gamma\right)\ . \quad (23\text{-}31)$$

The γ-dependent factor is also plotted in fig. 23.1. It is always positive, but mostly very small and vanishes like $\frac{1}{5}\gamma^2$ for $\gamma \to 0$. If the angle of attack α is positive, the positive moment tends to rotate the wing towards the horizontal, whereas for negative α the moment tends to turn the wing further into the ground.

Example 23.3.1: A completely flat unbent playing card thrown with a positive angle of attack will slowly sink further and further towards the table surface while the tiny moment rotates it towards the horizontal and the lift becomes still smaller (here we ignore again any forces acting on the upper side of the card). Thrown with a negative angle of attack, the playing card will get sucked towards the table at an increasing rate because the positive moment makes the angle of attack still more negative. Eventually, the card may catch on surface irregularities and turn over, showing its value to the dismay of the players.

Flow reversal

From the discharge rate (23-26) it follows that the equivalent planar flow height is

$$h_0 = \left(1-\gamma^2\right) d, \quad (23\text{-}32)$$

so that the condition for flow reversal (23-22) becomes

$$\gamma\frac{2x}{L} < \frac{3\gamma^2-1}{2}\ . \quad (23\text{-}33)$$

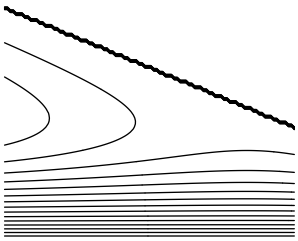

Flow reversal under flat wing moving towards the left with $\gamma = 0.7$. The samme pattern arises, if the wing moves towards the right with $\gamma = -0.7$.

For positive angle of attack, $\gamma > 0$, the condition is easiest to fulfill at the front of the wing for $x = -L/2$ where the left hand side is smallest. Solving the quadratic inequality, $-\gamma < (3\gamma^2-1)/2$, we find $\gamma > 1/3$. For sufficiently large positive angle of attack, there will always be flow reversal. Likewise, for sufficiently large negative angle of attack, a similar calculation shows that for $\gamma < -1/3$, there will also be flow reversal.

Copyright © 1998–2002, Benny Lautrup

23.4 Loaded journal bearing

In section 18.10 we discussed the case of laminar flow between two concentric rotating cylinders — the prototypical *journal bearing*. If the inner shaft or the outer sleeve (bushing) carries a load, the cylinders will no more be concentric but rather have their axes offset, though still parallel with respect to each other.

In a non-rotating journal bearing the lubricating fluid will be squeezed out and the shaft will come in direct contact with the sleeve. Whether the resting point of contact will be at the top or the bottom (with gravity pointing downwards) depends on whether it is the shaft or the sleeve that carries the load. When the shaft is brought into rotation, fluid will be dragged along due to the no-slip condition and forced into the narrow part of the gap, thereby creating a pressure that tends to lift the shaft away from the sleeve.

Intuitively, the pressure must be higher where the gap narrows than where it widens. This asymmetry of the pressure with respect to the point of closest approach makes the direction of the total lift force acting on the shaft parallel with the surface velocity at the point of closest approach, rather than orthogonal to it. When the shaft just starts to rotate, the direction of lift will thus be different from the direction of load, and with no other forces at play, the lift will tend to shift the shaft towards the side of the bushing, until it reaches a point where the direction of lift is opposite to the direction of the load. The end result is that the shaft is moved horizontally from its original position until the pressure in the gap has become so high that the vertical lift completely balances the load. This is the steady flow situation which we shall now study.

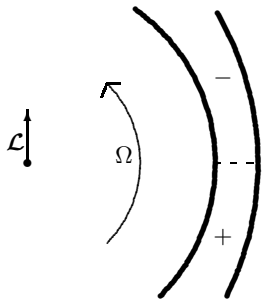

The pressure generated by the shaft's rotation is asymmetric with respect to the point of closest approach. The total lift $\mathcal{L}$ is always parallel with the direction of motion at the point of closest approach.

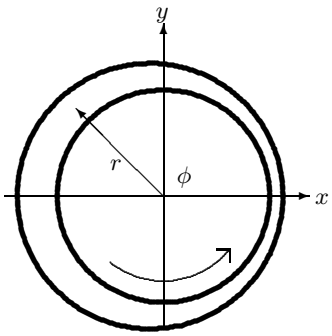

Geometry of off-center journal bearing with a vertical load pointing downwards along the y-axis. The inner cylinder has radius a and the outer b. The outer cylinder is shifted to the left by an amount c. The inner cylinder rotates with constant angular velocity Ω in the counter-clockwise direction.

Narrow gap approximation

Let the inner cylinder have radius a and the outer radius $b > a$ with a difference $d = b - a$ that is assumed to be tiny, $d \ll a$. In a coordinate system with the z-axis coinciding with the axis of the inner cylinder, the shift of the outer cylinder may without loss of generality be taken to be in the direction of negative x. The points of the outer cylinder are determined by the equation $(x + c)^2 + y^2 = b^2$ where c is the shift. In standard cylindrical (polar) coordinates this becomes $r^2 + c^2 + 2rc\cos\phi = b^2$, which to first order in c has the solution $r = b - c\cos\phi$. The width of the gap $h = r - a$ between the cylinders becomes

$$h(\phi) = d - c\cos\phi \ . \tag{23-34}$$

It is convenient to introduce the relative offset

$$\gamma = \frac{c}{d} \tag{23-35}$$

which is a dimensionless parameter that must lie in the interval $-1 \le \gamma \le 1$.

The shaft has length $L \gg a$ and rotates at constant angular velocity Ω with surface velocity $U = a\Omega$. Disregarding the possibility that lubricant may be squeezed out along the z-axis, the problem is essentially two-dimensional, such

Copyright © 1998–2002, Benny Lautrup

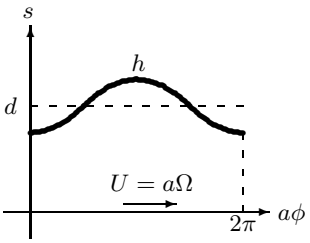

"Flattened" gap between the cylinders. The inner cylinder replaces the flat boundary along the x-axis with $x \to a\phi$, and the outer cylinder replaces the curved surface with $y \to s = r - a$. The 'ground' velocity of the inner cylinder is $U = a\Omega$

that the longitudinal field vanishes, $v_z = 0$, and the azimuthal and radial fields, v_ϕ and v_r, can only depend on r and ϕ, but not on z.

In this approximation, the general theory of flow in a narrow gap (section 23.2) may be brought into play, replacing x by $a\phi$ and y by $s = r - a$. The velocity components are

$$v_\phi = U\frac{(h-s)(h-3s)}{h^2} + Q\frac{6s(h-s)}{h^3} \ , \tag{23-36}$$

$$v_r = 2\alpha\left(\frac{U}{h^3} - \frac{3Q}{h^4}\right)s^2(h-s) \ . \tag{23-37}$$

The pressure can only depend on ϕ and from (23-15) we get

$$P'(\phi) = 6a\eta\left(\frac{U}{h(\phi)^2} - \frac{2Q}{h(\phi)^3}\right) \ . \tag{23-38}$$

Using that $P(2\pi) = P(0)$, we find (see problem 23.5) by integrating this expression over $0 \le \phi \le 2\pi$, the lubricant discharge rate per unit of shaft length

$$Q = Ud\,\frac{1-\gamma^2}{2+\gamma^2} \ . \tag{23-39}$$

For $\gamma = 0$ where the cylinders are concentric, this is the well-known result from Couette flow. In the other extreme $|\gamma| = 1$ where the cylinders touch, it vanishes, as one would expect.

Lift

Normalizing the pressure to vanish for $\phi = 0$, we may check by differentiation that the pressure is,

$$P(\phi) = -\frac{6\eta U a}{d^2}\ \frac{\gamma(2-\gamma\cos\phi)\sin\phi}{(2+\gamma^2)(1-\gamma\cos\phi)^2} \ . \tag{23-40}$$

If $\gamma > 0$, the pressure is positive for $\phi < 0$ and negative for $\phi > 0$. The total pressure force on the inner cylinder is a vector

$$\boldsymbol{\mathcal{L}} = (\mathcal{L}_x, \mathcal{L}_y) = \oint_{r=a}(-p)\,d\boldsymbol{S} = -\int_0^{2\pi} P(\phi)(\cos\phi, \sin\phi)\,Lad\phi \ . \tag{23-41}$$

It follows explicitly from the symmetry of the pressure that $\mathcal{L}_x = 0$, whereas (see problem 23.4)

$$\mathcal{L}_y = \frac{6\pi\eta\Omega a^3 L}{d^2}\ \frac{2\gamma}{(2+\gamma^2)\sqrt{1-\gamma^2}} \ . \tag{23-42}$$

Since the area of the shaft is $A = 2\pi aL$, this expression is of the same general form as the estimate (23-4), and positive for $\gamma > 0$, as expected.

The behavior of the γ-dependent factor in (23-42) is shown in fig. 23.2. It is nearly linear in the interval $-0.9 < \gamma < 0.9$, outside which it diverges rapidly. This divergence permits the bearing to carry any size load by adjusting γ to be sufficiently close to unity. But there is a price to pay, as we shall now see.

Copyright © 1998–2002, Benny Lautrup

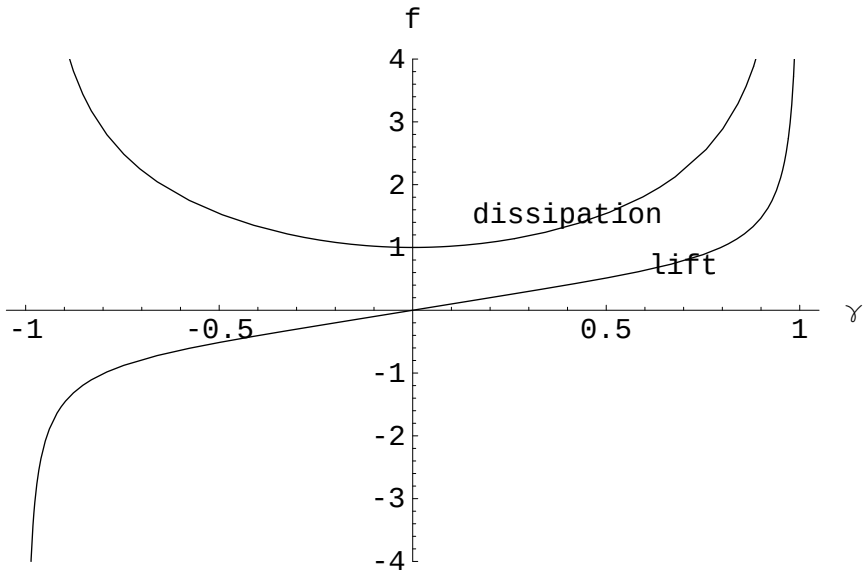

Figure 23.2: *Orientation-dependent shape factors for lift and dissipation for a journal bearing as a function of the relative center offset, $\gamma = c/d$. Both quantities diverge as an inverse squareroot for $|\gamma| \to 1$.*

Drag moment and dissipation

The shear stress at the surface of the shaft is

$$\sigma_{\phi r} \approx \eta \left.\frac{\partial v_\phi}{\partial s}\right|_{s=0} = -2\eta \left(\frac{2U}{h} - \frac{3Q}{h^2}\right) . \tag{23-43}$$

The total moment of shear stress around the center of the shaft becomes (problem 23.5)

$$\mathcal{M} = \int_0^{2\pi} a\sigma_{\phi r} L a d\phi = -\frac{2\pi\eta U L a^2}{d} \frac{2}{\sqrt{1-\gamma^2}} \frac{1+2\gamma^2}{2+\gamma^2} . \tag{23-44}$$

It is negative as one would expect and the rate of work performed by the external forces is obtained by multiplying with $-\Omega$,

$$P = \frac{2\pi\eta\Omega^2 a^3 L}{d} \frac{2}{\sqrt{1-\gamma^2}} \frac{1+2\gamma^2}{2+\gamma^2} . \tag{23-45}$$

For $\gamma \to 0$ the dissipated power approaches the result for the unloaded bearing (18-65), whereas for $|\gamma| \to 1$ it diverges (like lift) as an inverse squareroot. The large heat dissipation in heavily loaded journal bearings can be avoided by employing rollers or balls to keep the shaft centered in the bushing.

The ratio of dissipated power to lift,

$$\frac{P}{\mathcal{L}_y} = \frac{1+2\gamma^2}{\gamma} \Omega d , \tag{23-46}$$

Copyright © 1998–2002, Benny Lautrup

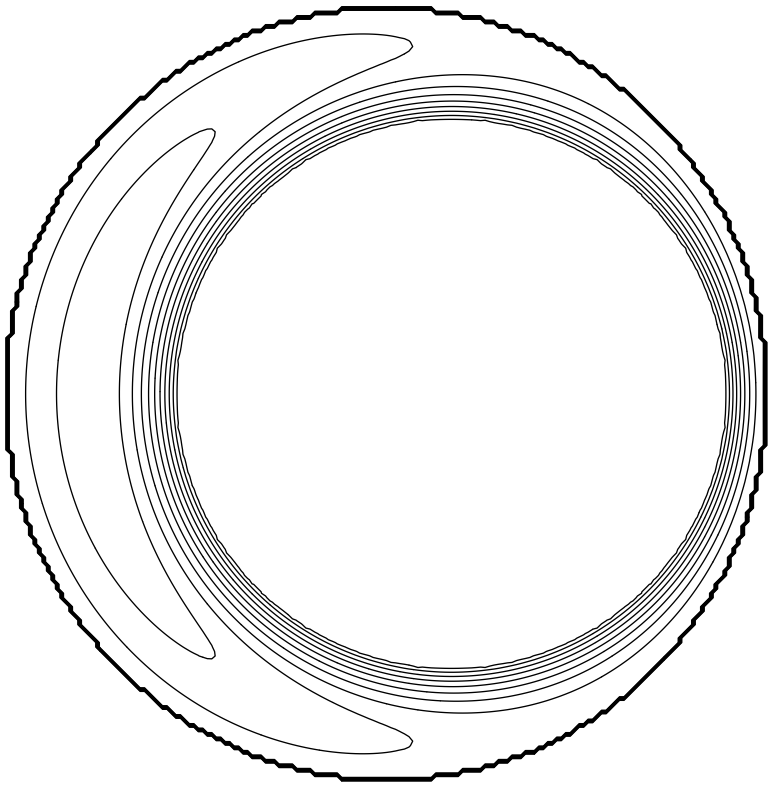

Figure 23.3: *Creeping flow pattern in loaded journal bearing with* $d/a = 0.4$ *and* $\gamma = 0.6$. *Notice the reversed flow, in the form of a counter-rotating roller, near* $\phi = \pi$.

is finite for $|\gamma| \to 1$. Since a heavily loaded bearing has $|\gamma| \approx 1$, the ratio becomes $P/\mathcal{L}_y \approx 2\Omega d$ in this limit, and since the lift must equal the load, this makes it easy to calculate the dissipated power.

Flow reversal

The narrow gap between the cylinders looks like a flat gap with a widening bump opposite the point of closest contact. The discussion in section 23.2 leads to the expectation that there will arise a stationary flow-reversing "roller" at this point (see fig. 23.4). The equivalent planar flow gap is obtained from (23-39),

$$h_0 = 2d\,\frac{1-\gamma^2}{2+\gamma^2}\ , \tag{23-47}$$

so that the general condition (23-22) becomes

$$1 - \gamma\cos\phi > 3\frac{1-\gamma^2}{2+\gamma^2}\ . \tag{23-48}$$

The left hand side is (for positive γ) largest for $\phi = \pi$, as expected. Solving the inequality $1 + \gamma > 3(1-\gamma^2)/(2+\gamma^2)$, we obtain $\gamma > (\sqrt{13} - 3)/2 \approx 0.303$.

Copyright © 1998–2002, Benny Lautrup

Problems

23.1 Find the critical gap height for creeping flight when the shape factor is $f = \alpha L/2d$ where α is the constant angle of attack.

23.2 Show explicitly that the fluid discharge rate Q (eq. (23-14) is independent of x.

23.3 Find the conditions on the discharge rate under which the velocity (23-16) has an extreme in the gap (as a function of y).

23.4 Show that

$$\int_0^{2\pi} P(\phi)\sin\phi\, d\phi = \int_0^{2\pi} P'(\phi)\cos\phi\, d\phi \tag{23-49}$$

and use the integrals of problem 23.5

∗ **23.5** Show that for $|\gamma| < 1$

$$\int_0^{2\pi} \frac{1}{1-\gamma\cos\phi}\frac{d\phi}{2\pi} = \frac{1}{\sqrt{1-\gamma^2}}$$

$$\int_0^{2\pi} \frac{1}{(1-\gamma\cos\phi)^2}\frac{d\phi}{2\pi} = \frac{1}{(1-\gamma^2)^{\frac{3}{2}}}$$

$$\int_0^{2\pi} \frac{1}{(1-\gamma\cos\phi)^3}\frac{d\phi}{2\pi} = \frac{2+\gamma^2}{2(1-\gamma^2)^{\frac{5}{2}}}$$

$$\int_0^{2\pi} \frac{\cos\phi}{(1-\gamma\cos\phi)^2}\frac{d\phi}{2\pi} = \frac{\gamma}{(1-\gamma^2)^{\frac{3}{2}}}$$

$$\int_0^{2\pi} \frac{\cos\phi}{(1-\gamma\cos\phi)^3}\frac{d\phi}{2\pi} = \frac{3\gamma}{2(1-\gamma^2)^{\frac{5}{2}}}$$

Copyright © 1998–2002, Benny Lautrup

Copyright © 1998–2002, Benny Lautrup